Electronic Supplementary Information

Experimental

Materials: Hydrazine ($N_2H_4 \cdot H_2O$), ammonium fluoride (NH_4F), Nitric acid (HNO_3), Sulfuric acid (H_2SO_4), hydrochloric acid (HCl), and ethanol (C_2H_5OH) were purchased from Chengdu Kelong Chemical Reagent Factory. Salicylic acid ($C_7H_6O_3$), ammonium chloride (NH_4Cl), Ethylene Diamine Tetraacetic Acid (EDTA), *p*-dimethylaminobenzaldehyde ($C_9H_{11}NO$), sodium citrate dehydrates ($C_6H_5Na_3O_7 \cdot 2H_2O$), sodium nitroferricyanide dihydrate ($C_5FeN_6Na_2O \cdot 2H_2O$), $FeSO_4$, and sodium hypochlorite solution (NaClO) were purchased from Beijing Chemical Corp. (China). All the reagents were used as received without further purification. A mixed gas of NO/Ar (10 *vol.*% NO) was purchased from Yinde City Xizhou Gas Co., Ltd (China). Ti mesh (TM) was purchased from Hongshan District, Wuhan Instrument Surgical Instruments business and was pretreated in HNO_3, then was cleaned by sonication sequentially in acetone, H_2O, and C_2H_5OH several times to remove the surface impurities. The water used throughout all experiments was purified through a Millipore system.

Synthesis of Ni(OH)$_2$/TM: 1.4 mmol $Ni(NO_3)_2 \cdot 6H_2O$, 2.7 mmol NH_4F, and 7 mmol UREA and a piece of Ti mesh (2cm * 2cm) were dissolved in 35 ml H_2O. Then put this mixture into the reactor made by Teflon. After reaction for 8 h at 100°C collected the Ti mesh washed with EtOH and H_2O several times. The $Ni(OH)_2$/TM was dried under vacuum at 60°C overnight.

Synthesis of NiO/TM: The $Ni(OH)_2$/TM was used as a precursor for annealing in a tube furnace at 350°C in the air for 180 min. After the cooling to room temperature, The NiO/TM was washed three times with deionized water. The NiO/TM was totally dried under vacuum at 60°C overnight.

Characterizations: SEM (Zeiss Gemni SEM 300) and TEM (FEI TF200) were adopted to characterize the morphology and structure of as-synthesized samples. The crystal phases of the samples were evaluated through the XRD (Philips PW1730). XPS (Thermo ESCALAB 250XI) adopting Mg as the excitation source and EDX elemental mapping images were carried out to investigate the chemical composition and element distribution of the samples.

Electrochemical measurement: NO reduction experiments were carried out in a two-compartment cell under ambient conditions, which was separated by the Nafion

117 membrane. The Nafion 117 membrane was pretreated with 5% H_2O_2 solution and 10% H_2SO_4 for 1 h at 80°C, respectively, and deionized water for another 1 h. Electrochemical data were collected with a CHI 660E electrochemical workstation. Three electrode system was used in the electrochemical measurement and the three electrodes arrangement consisted of a graphite rod as the counter electrode, Ag/AgCl (saturated KCl electrolyte) as the reference electrode. The NiO/TM can be directly used as a working electrode. All potentials were referenced against the reversible hydrogen electrode (RHE) based on the Nernst equation ($E_{RHE} = E_{SCE} + 0.059 \times pH + 0.197$). For NO reduction experiments, the chronoamperometry test was conducted in NO saturated 0.10 M Na_2SO_4 + 0.05 mM Fe-EDTA solution (50 mL) (the electrolyte was purged with Ar for 10 min before the measurement.). NO/Ar mixture gas was introduced to the cathodic compartment using properly positioned spargers so that the whole cathode was hit by the gas bubbles.

Determination of NH_3: The yield of the NH_3 was determined by a spectrophotometry measurement with the indophenol blue method. In detail, 4 mL electrolyte was obtained from the cathodic chamber and mixed with 50 µL oxidizing solution containing NaClO (4.5%) and NaOH (0.75 M), 500 µL coloring solution containing $C_7H_5O_3Na$ (0.4 M) and NaOH (0.32 M), and 50 µL catalyst solution $Na_2Fe(CN)_5NO{\cdot}2H_2O$ (1 wt%) for 1 h. The concentration-absorbance curve was calibrated using the standard NH_4Cl solution with NH_3 concentrations of 0, 0.1, 0.2, 0.3, 0.4, 0.5, and 1.0 µg mL^{-1} in 0.1 M Na_2SO_4. These solutions were identified via UV-Vis spectroscopy at the wavelength of 660 nm. The concentration-absorbance curves were calibrated using a standard NH_3 solution with a series of concentrations. The fitting curve ($y = 0.53x + 0.021$, $R^2 = 0.9999$) shows good linear relation of absorbance value with NH_3 concentration.

Determination of N_2H_4: A mixed solution of 1.97 g $C_9H_{11}NO$, 10 mL concentrated HCl and 100 ml ethanol was used as a color reagent. The calibration curve was plotted as follow: firstly, preparing a series of N_2H_4 solutions of known concentration as standards; secondly, adding 4 mL color reagent into above N_2H_4 solution separately, and standing 20 min at room temperature; finally, the absorbance of the resulting solution was measured at 460 nm in 10 mm glass cuvette by the UV-Vis-NIR spectrophotometer. The fitting curve shows good linear relation of absorbance with N_2H_4 concentration ($y = 0.8315x + 0.00214$, $R^2 = 0.999$).

Determination of NO_3^-: Firstly, a certain amount of electrolyte was taken out from the electrolytic cell and diluted to 5 mL to the detection range. Then, 0.1 mL 1 M HCl and 0.01 mL 0.8 wt% sulfamic acid solution were added into the aforementioned solution. The absorption spectrum was measured using a UV-Vis spectrophotometer and the absorption intensities at a wavelength of 220 nm and 275 nm were recorded. The final absorbance value was calculated by this equation: $A = A_{220\ nm} - 2A_{275\ nm}$. The concentration-absorbance curve was calibrated using a series of standard $NaNO_3$ solutions and the $NaNO_3$ crystal was dried at 110 ºC for 2 h in advance.

Determination of FE and NH_3 yield: The Faradaic efficiency for NORR was defined as the quantity of electric charge used for synthesizing ammonia divided by the total charge passed through the electrodes during the electrolysis. The yield of produced NH_3 was measured by the colorimetric method. From the reaction equation, it can be seen that the formation of one ammonia molecule requires three electrons, the Faradaic efficiency can be calculated as follows:

$$FE = n * F * [NH_3] * V / (17 * Q) * 100\% \quad (1)$$

where F is the Faraday constant, Q is the total quantity of applied electricity; t is the reduction time, n is the number of electrons was needed to produce one product molecule.

The rate of ammonia formation was calculated as follows:

$$NH_3 \text{ yield} = ([NH_3] * V) / (t * S) \quad (2)$$

Where $[NH_3]$ is the NH_3 concentration, V is the volume of electrolyte, t is the NRR time and S is the catalyst electrode area.

Zn-NO battery: A NiO nanosheet-loaded carbon paper electrode was employed as the cathode to perform the NORR in a cathodic electrolyte (0.1 M Na_2SO_4). A polished Zn plate was set in an anodic electrolyte (1 M NaOH), and a bipolar membrane was used to separate the two different electrolytes. During the battery discharge process, the Zn-NO electrochemistry implements electrochemical NO reduction driven by Zn dissolution, the electrochemical reactions on each electrode can be described as follows:

$$\text{Cathode: } NO + 4H_2O + 5e^- \rightarrow NH_3 + 5\ OH^- \quad (3)$$

$$\text{Anode: } Zn + 2OH^- \rightarrow ZnO + H_2O + 2e^- \quad (4)$$

$$\text{Overall: } 5Zn + 2NO + 3H_2O \rightarrow 5ZnO + 2NH_3 \quad (5)$$

Zn-NO battery potentially has a higher voltage output than that of the O_2-based cells, namely, metal-air batteries (as displayed in Table S3).

Calculation details: First-principles calculations with spin-polarized were performed based on density functional theory (DFT) implemented in the VASP package,[1] and the interaction between valence electrons and ionic core was expanded using the projector augmented wave (PAW) approach with a cutoff of 450 eV.[2] Perdew-Burke-Ernzerhof functional (PBE) with semi-empirical corrections of DFT-D3 was adopted to describe exchange-correlation functional effect based on general gradient approximation (GGA). 2 × 2 NiO (200) surface with four layers were modeled, for which the bottom two layer was fixed and the upper two layers were allowed to relax.[3] The thickness of the vacuum region is > 15 Å to avoid the spurious interaction. Hubbard U model was implemented with an effective U = 6.2 eV for Ni 3d orbitals. The Brillouin zone was sampled by 3 × 3 × 1 special k-points using the Monkhorst Pack scheme for structural configuration optimizations.[4] The force convergence thresholds are 0.02 eV/Å and the total energy less than $1E^{-5}$ eV, respectively. The theoretical calculation results were processing and analyzed by VASPKIT software.[5]

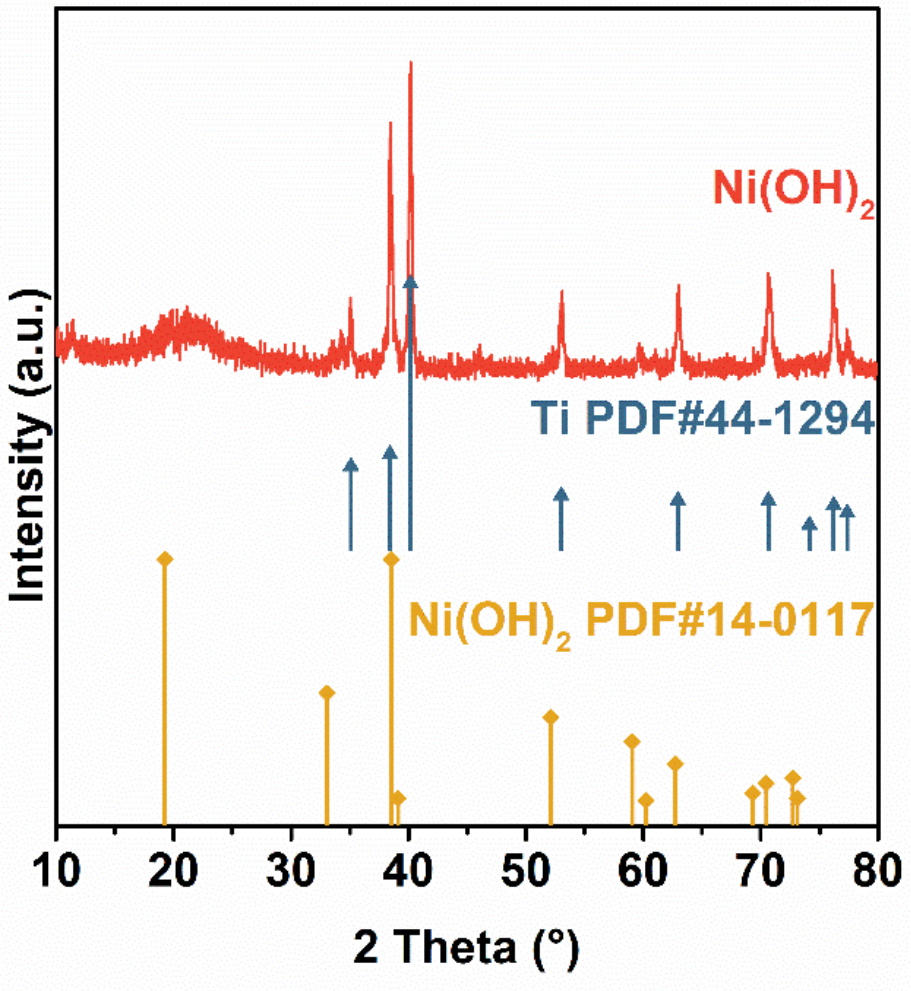

Fig. S1. XRD pattern of $Ni(OH)_2$/TM.

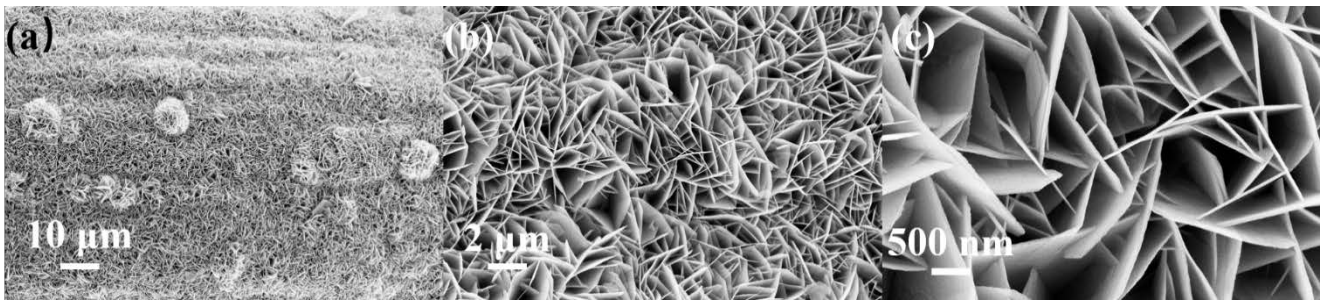

Fig. S2. (a-c) SEM images of $Ni(OH)_2$/TM.

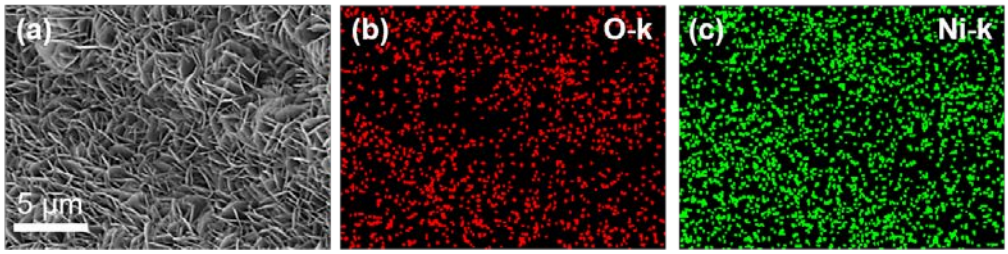

Fig. S3. (a) SEM image and corresponding EDX elemental mapping images of (b) O and (c) Ni for NiO/TM.

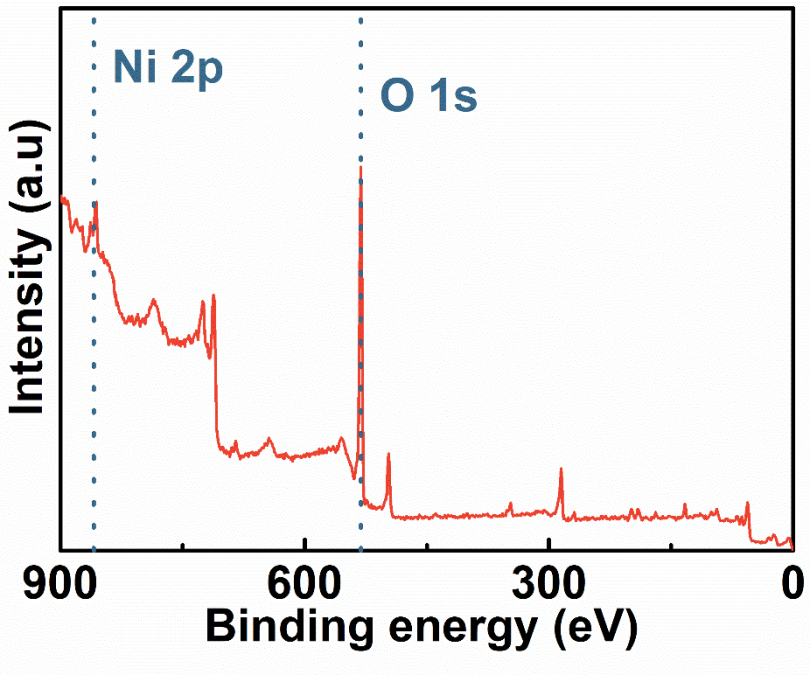

Fig. S4. XPS survey spectrum of NiO/TM.

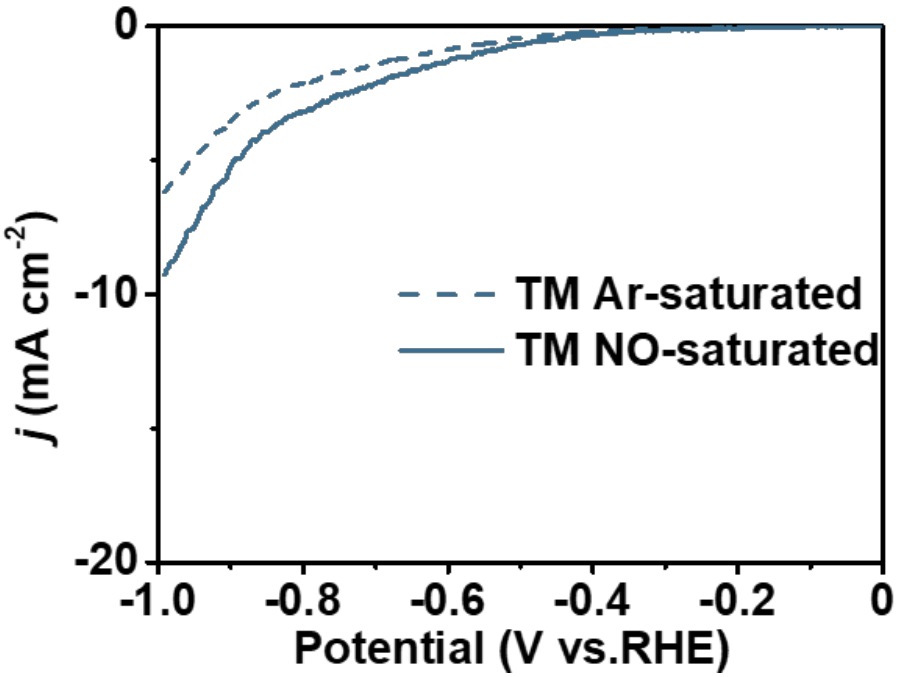

Fig. S5. LSV curves of TM in NO- and Ar-saturated 0.1 M Na_2SO_4 (scan rate: 5 mV s^{-1}).

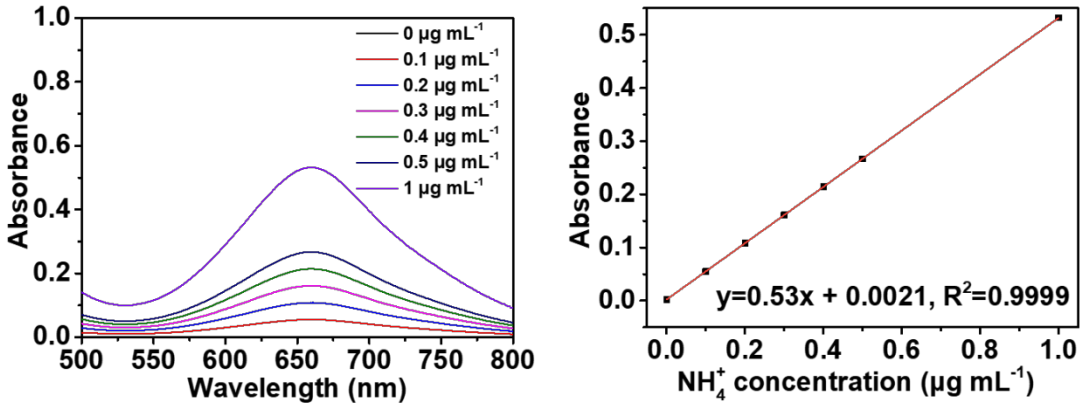

Fig. S6. (a) UV-Vis absorption spectra of indophenol assays with NH_3 after incubated for 1 h at room temperature and corresponding (b) calibration curve used for estimating NH_3.

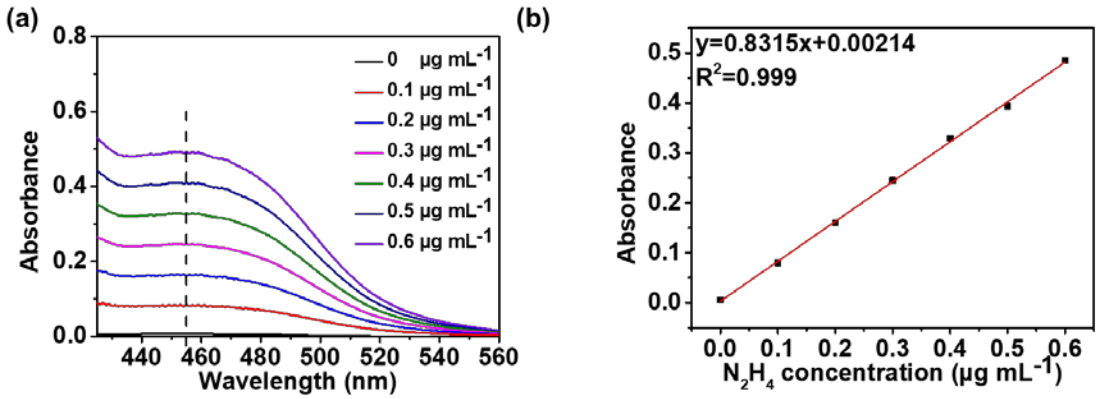

Fig. S7. (a) UV-Vis absorption spectra of various N_2H_4 concentration after incubated for 15 min at room temperature and corresponding (b) calibration curve used for estimating N_2H_4.

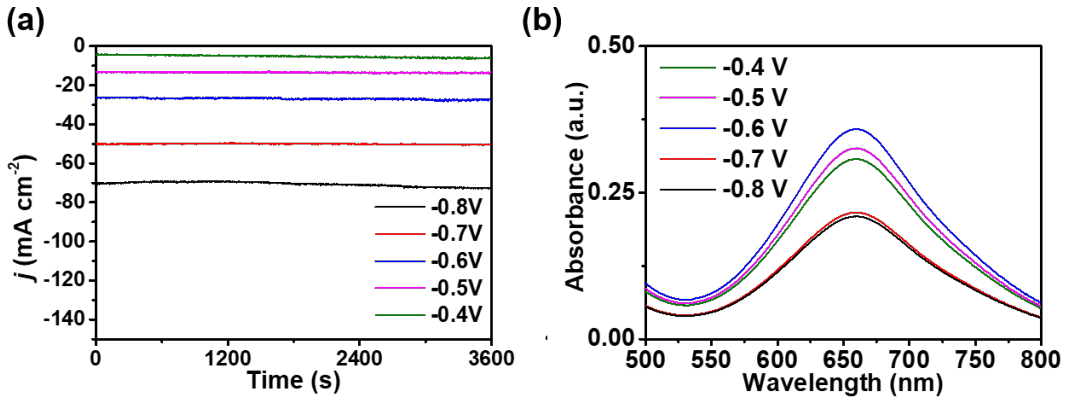

Fig. S8. (a) Time-dependent current density curves (1 h) for NiO/TM in NO-saturated 0.1 M Na_2SO_4 with 0.05 mM Fe-EDTA at various potentials. (b) Corresponding UV-vis absorption spectra of the electrolytes stained with indophenol indicator. (1:10).

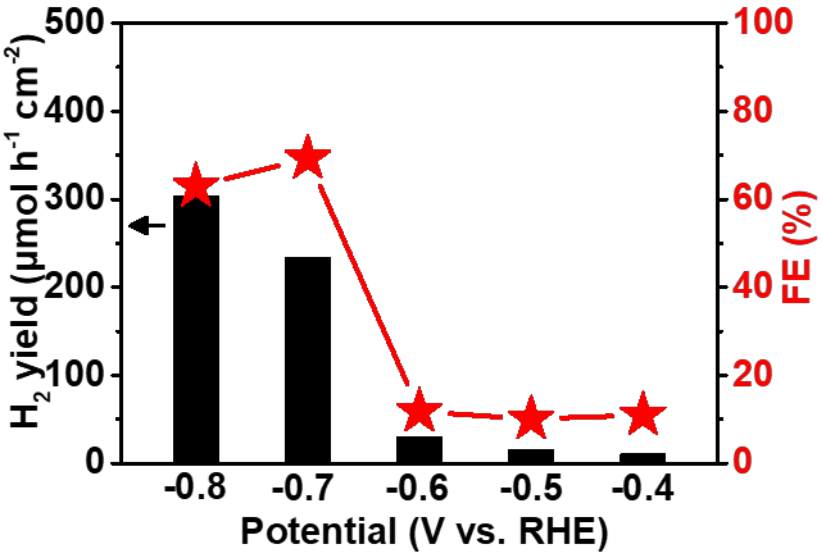

Fig. S9. NH_3 yields and FEs for NiO/TM of NORR at various potentials

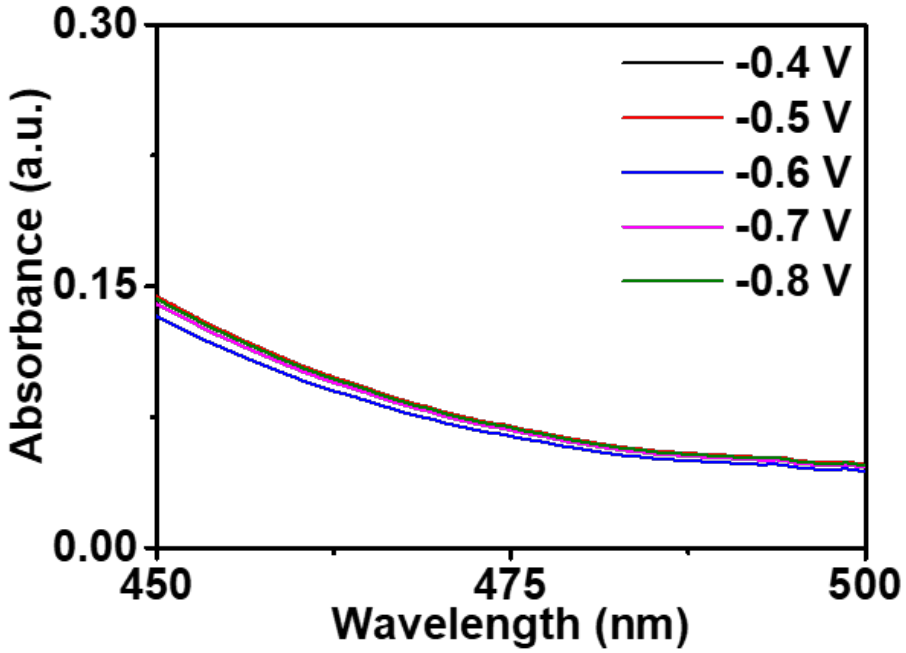

Fig. S10. UV-Vis absorption spectra of electrolytes estimated by the method of Watt and Chrisp after 1 h electrolysis on NiO/TM at each given potential.

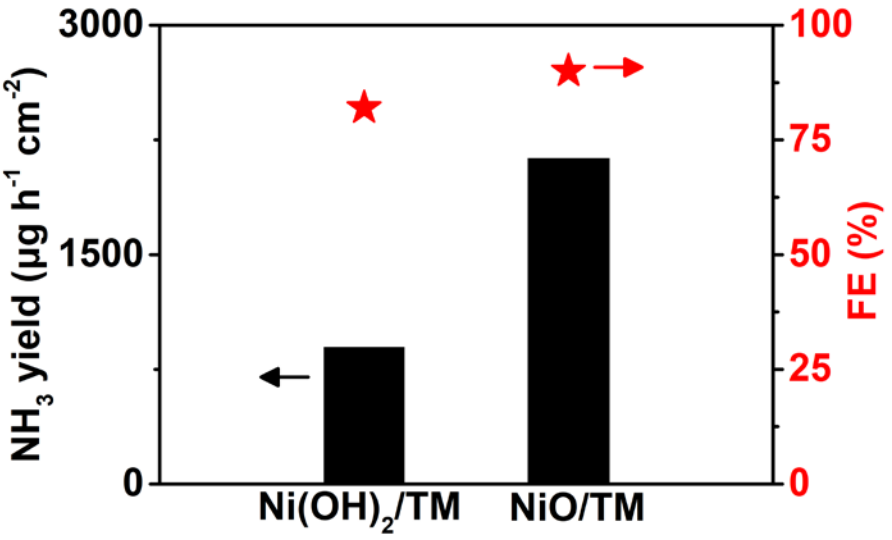

Fig. S11. FEs and yields of NH_3 for $Ni(OH)_2$/TM and NiO/TM at −0.6 V.

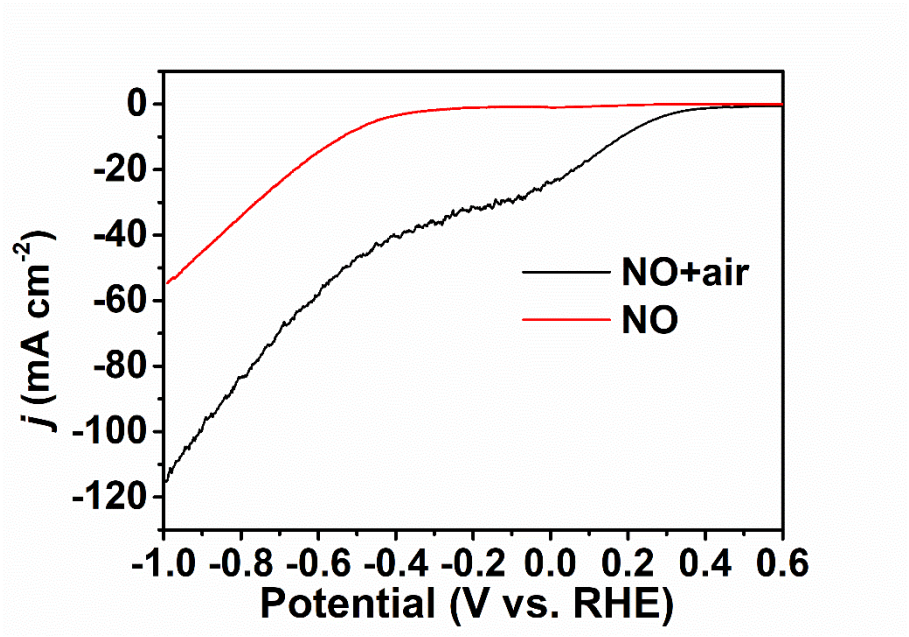

Fig. S12. LSV curves of NiO/TM in gas-tight（NO-saturated electrolyte) and open electrolytic cells (NO + air atmosphere).

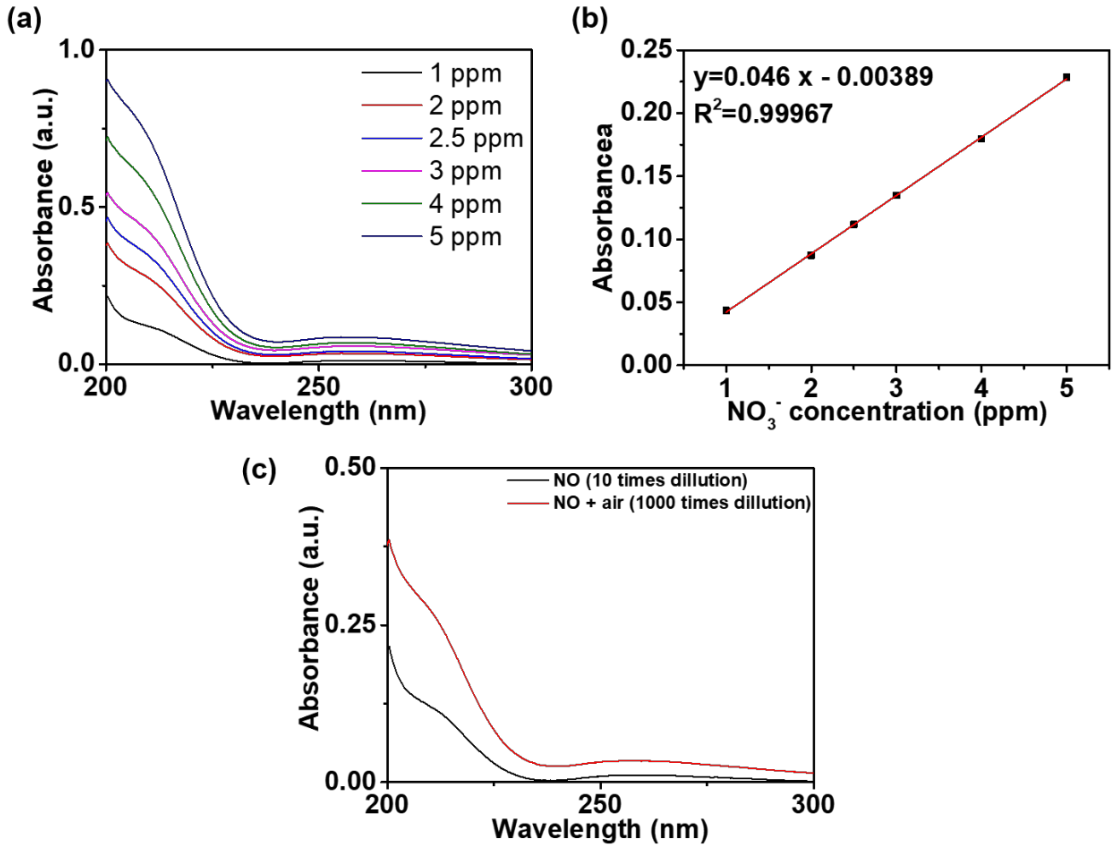

Fig. S13. (a) UV-Vis absorption spectra of various NO_3^-concentration after incubated for 20 min at room temperature and corresponding (b) calibration curve used for estimating NO_3^-. (c) UV-Vis absorption spectra of NO_3^- for NiO/TM in a gas-tight (in NO-saturated electrolyte) and open chambers (under NO + air atmosphere) at −0.6 V after 1 h electrolysis.

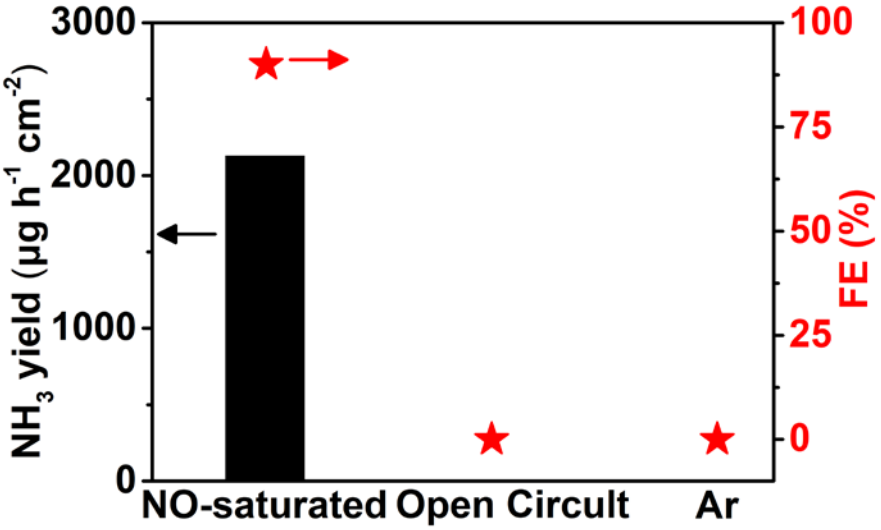

Fig. S14. NH_3 yields and FEs of NiO/TM under different conditions.

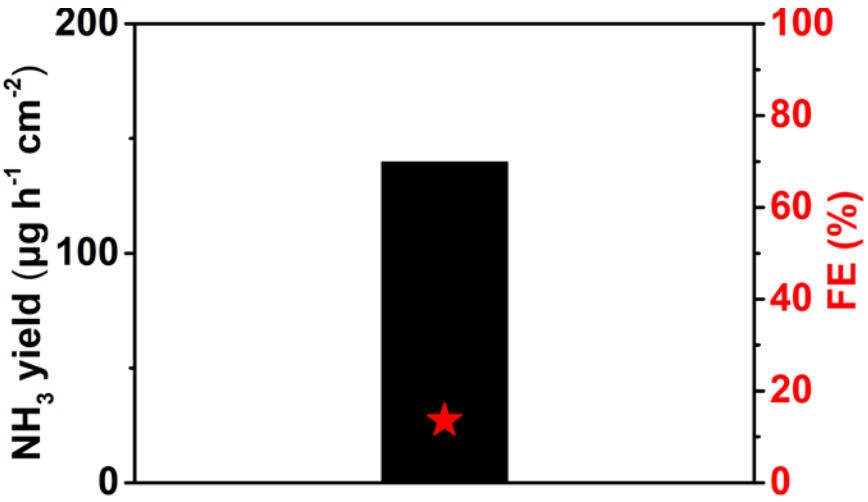

Fig. S15. NH_3 yield and FE of NORR on TM.

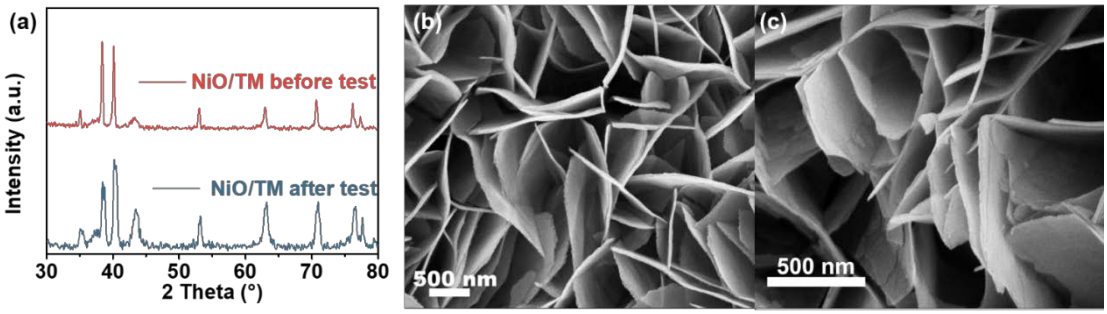

Fig. S16. (a) XRD patterns of NiO/TM before and after test. (b) SEM image of NiO/TM. (c) SEM image of post-electrolysis NiO/TM.

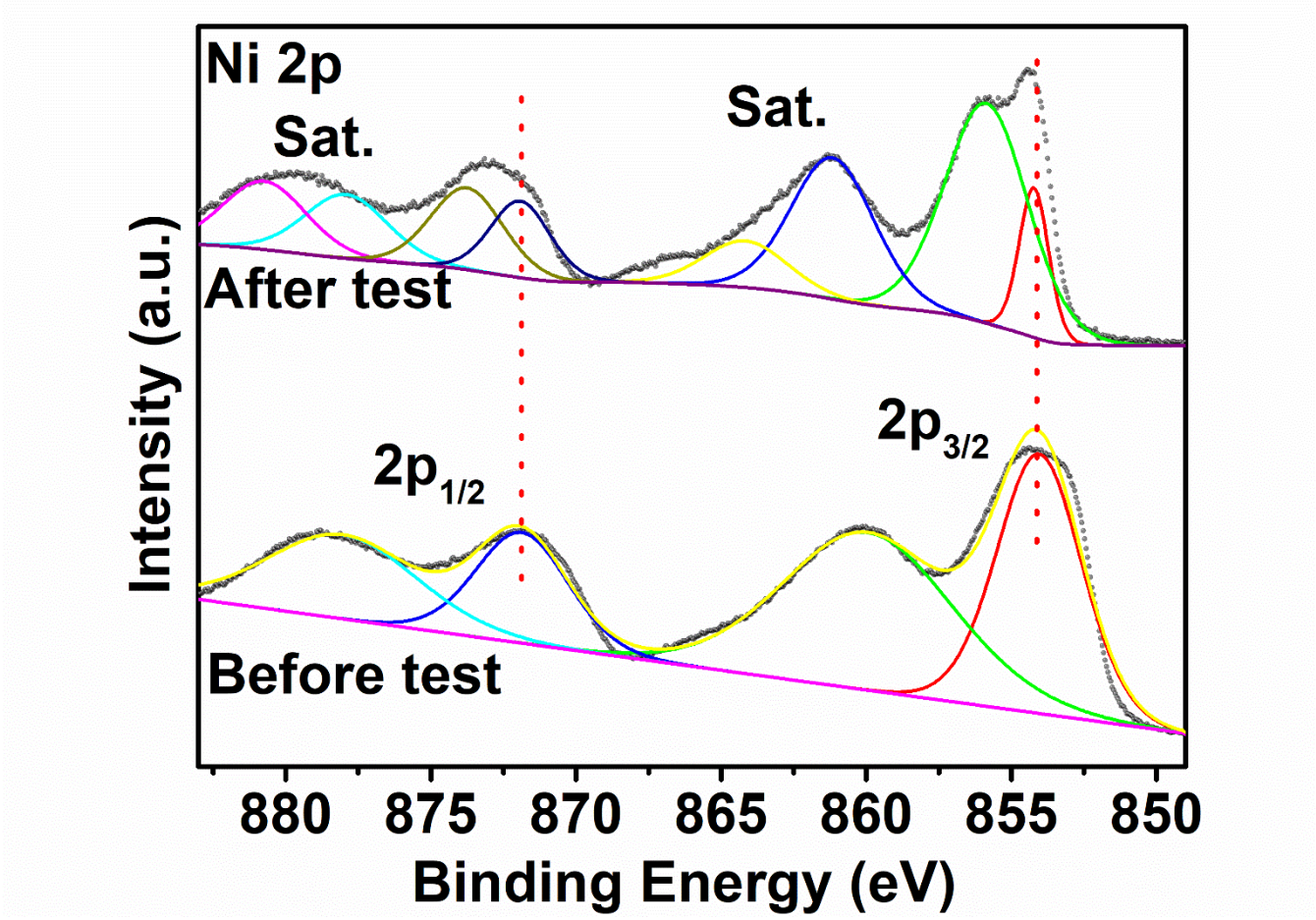

Fig. S17. XPS spectra of NiO/TM in Ni 2p region before and after electrolysis test.

The shoulder peaks in NiO/TM after test presented at 855.8 eV and 873.7 eV are derived from the Ni^{2+} species on the surface.[6,7] And the peaks of Ni^{2+} in the NiO/TM after test at 871.7 eV and 854.3 eV didn't show any shift after electrolysis test.

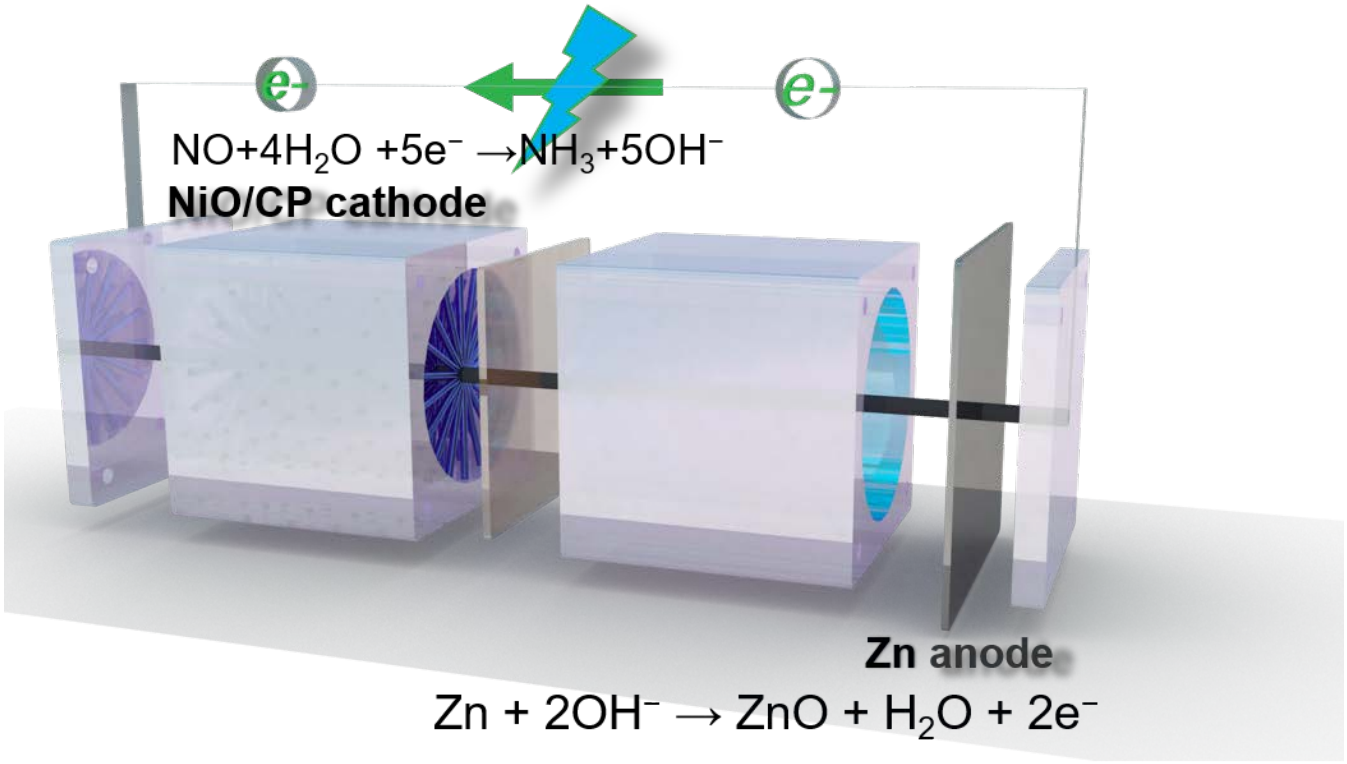

Fig. S18. Schematic of Zn-NO battery.

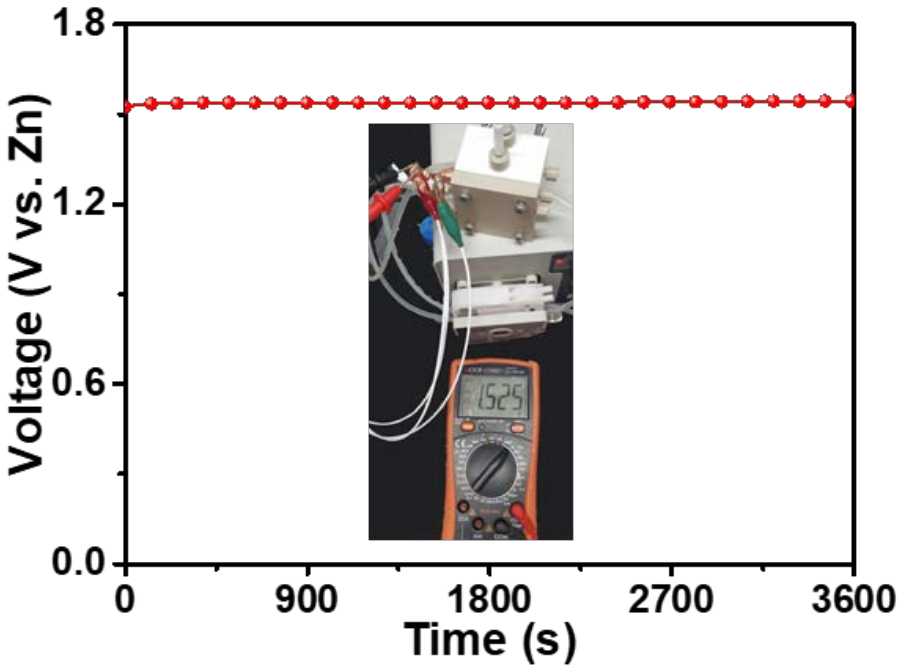

Fig. S19. Open-circuit voltage of the Zn-NO battery with the NiO/CP catalyst cathode.

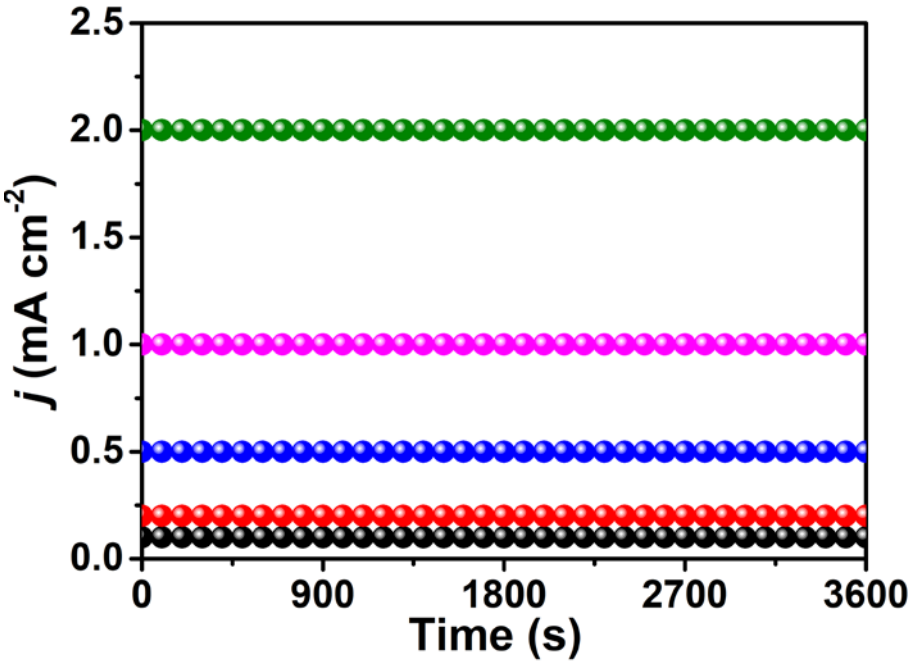

Fig. S20. Time-dependent current density curves of Zn-NO battery.

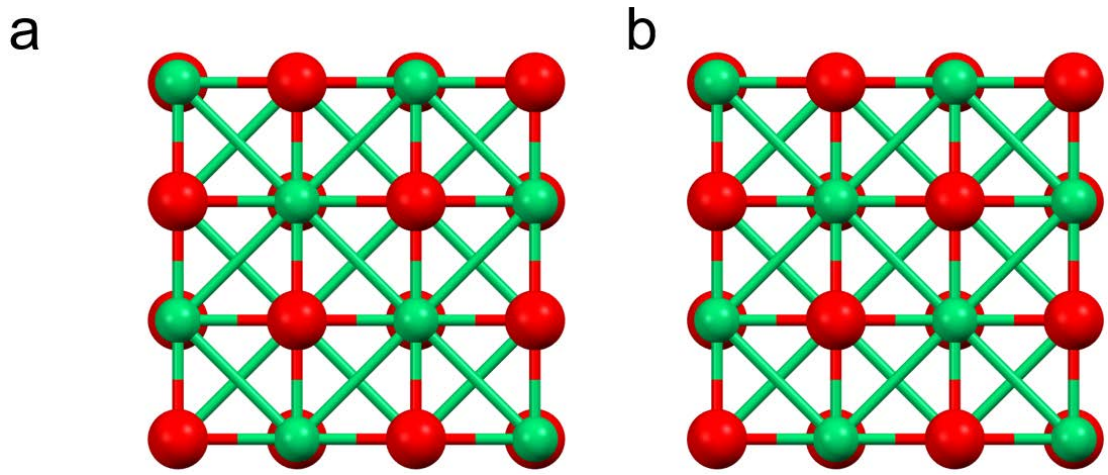

Fig. S21. (a) Top and (b) side views of the NiO (200) slab models. Green and red spheres represent Ni and O atoms, respectively.

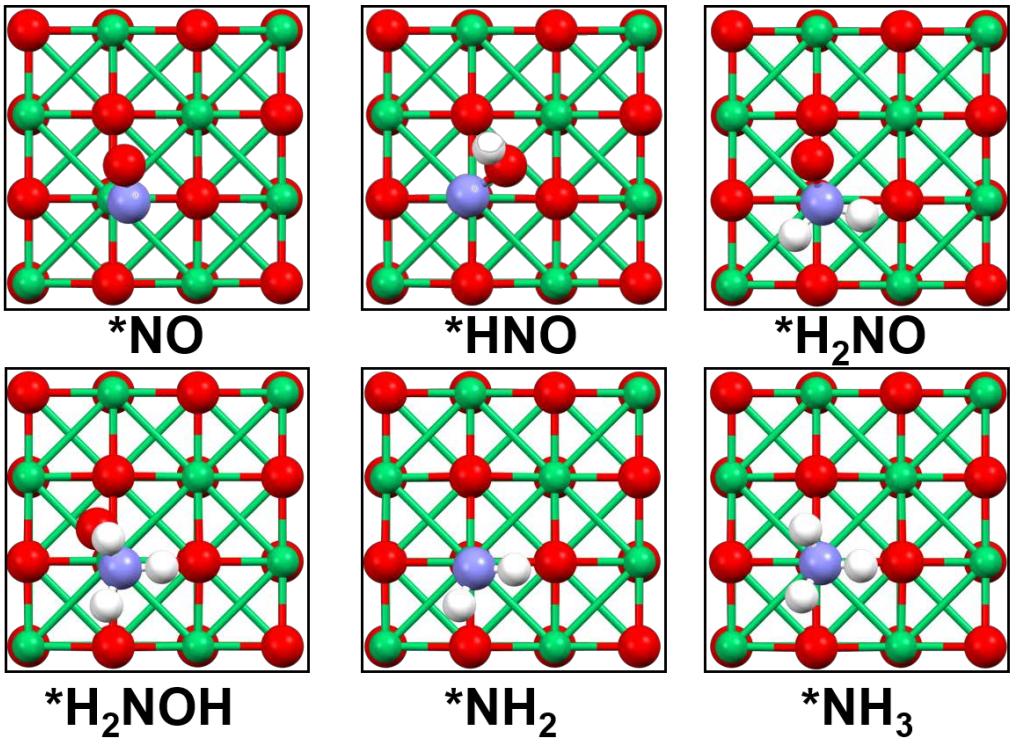

Fig. S22. Atomic structures of the corresponding intermediates. Green, red, blue, and white spheres represent Ni, O, N, and H atoms, respectively.

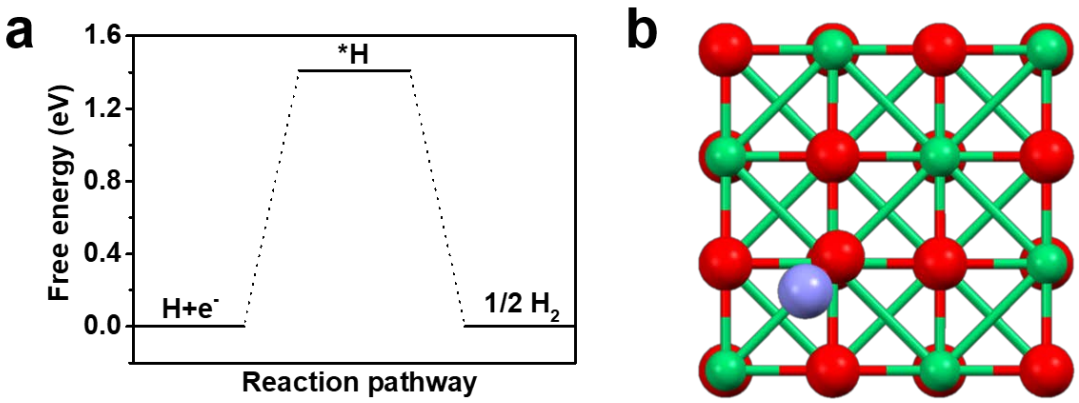

Fig. S23. (a) Free energy diagram of HER. (b) Top views of the NiO (200) with H atom slab models, blue sphere represents H atom.

Table S1. Comparison of NH_3 yields and FEs of NiO/TM with reported aqueous-based NRR and NORR electrocatalysts.

Catalysts	Electrolyte	NH_3 yield	FE (%)	Potential (vs. RHE)	Ref.
NiO/TM	0.1 M Na_2SO_4 + 0.05 mM Fe^{2+}-EDTA	2130 μg h^{-1} cm^{-2}	90	−0.6 V	This work
$PdBi_2$	0.05 M H_2SO_4	59.05 μg h^{-1} $mg_{cat.}^{-1}$	21.5	−0.2 V	*Adv. Mater.*, 2021, **33**, 2007733
CuS	0.1 M HCl	18.18 μg h^{-1} $mg_{cat.}^{-1}$	5.6	−0.15 V	*Inorg. Chem. Front.*, 2021, **8**, 3105−3110
MXene/$TiFeO_x$-700	0.05 M H_2SO_4	2.19 μg cm^{-2} h^{-1}	25.4	−0.2 V	*ACS Nano*, 2020, **14**, 9089−9097
NbS_2	0.1 M HCl	37.58 μg h^{-1} mg^{-1}	10.1	−0.5 V	*Appl. Catal. B: Environ.*, 2020, **270**, 118892
Bi_2MoO_6	0.1 M HCl	20.46 μg h^{-1} $mg_{cat.}^{-1}$	8.1	–0.6 V	*ACS Sustain. Chem. Eng.*, 2019, **7**, 12692−12696
Au_6/Ni	0.05 M H_2SO_4	7.4 μg h^{-1} $mg_{cat.}^{-1}$	67.8	–0.14 V	*J. Am. Chem. Soc.*, 2019, **141**, 14976−14980
MoO_2	0.1 M HCl	12.2 μg h^{-1} $mg_{cat.}^{-1}$	8.2	–0.15 V	*Nano Energy*, 2019, **59**, 10−16
Ru/MoS_2	0.01 M HCl	7.0 μg h^{-1} $mg_{cat.}^{-1}$	17.6	–0.15 V	*ACS Energy Lett.*, 2019, **4**, 430−435
B_4C	0.1 M HCl	26.57 μg h^{-1} $mg_{cat.}^{-1}$	16.1	–0.75 V	*Nat. Commun.*, 2018, **9**, 3485
MoS_2	0.1 M HCl	2.9 μmol cm^{-2} h^{-1}	1.2	–0.5 V	*Adv. Mater.*, 2018, **30**, 1800191
VN nanoparticles	1 mM H_2SO_4	1.18 μmol cm^{-2} h^{-1}	6.1	–0.1 V	*J. Am. Chem. Soc.*, 2018, **140**, 13387−13391
Ru SAs/N-C	0.05 M H_2SO_4	1.8 μmol cm^{-2} h^{-1}	29.6	–0.2 V	*Adv. Mater.*, 2018, **30**, 1803498
Au	0.01 M HCl	25.57 μg h^{-1} $mg_{cat.}^{-1}$	6.0	–0.2 V	*ChemSusChem*, 2018, **11**, 3480

Ag nanosheet	0.1 M HCl	0.164 μmol cm^{-2} h^{-1}	4.8	–0.6 V	*Chem. Commun.*, 2018, **54**, 11427–11430
$CoSe_2$@CNTs (NORR)	Fe(II)EDTA + Na_2SO_4	/	48.1	2.5 V	*Environ. Sci. Pollut. Res.*, 2017, **24**, 14249–14258
$Ru_{0.05}Cu_{0.95}$(NORR)	0.5 M Na_2SO_4	17.68 μmol cm^{-2} h^{-1}	64.9	–0.5 V	*Sci. China. Chem.*, 2021, **64**, 1493–1497
Cu foam (NORR)	0.25 M Li_2SO_4	517.1 μmol cm^{-2} h^{-1}	93.5	–0.9 V	*Angew. Chem., Int. Ed.*, 2020, **59**, 9711–9718
Cu foil (NORR)	0.25 M Li_2SO_4	95.0 μmol cm^{-2} h^{-1}	61.9		
Pt foil (NORR)	0.25 M Li_2SO_4	99.4 μmol cm^{-2} h^{-1}	24.1		
Single atom Nb (NORR)	0.1 M HCl	295.2 μmol cm^{-2} h^{-1}	77.1	–0.6 V	*Nano Energy*, 2020, **78**, 105321
FeNC (NORR)	0.1 M $HClO_4$	~20.2 μmol cm^{-2} h^{-1}	~5.1	–0.2 V	*Nat. Commun.*, 2021, **12**, 1856
Ag	0.5 M PBS + 50 mM EFeMC	0.28 mol m^{-2} h^{-1}	~100	−0.165 V	*ACS Energy Lett.*, 2020, **5**, 3647-3656
MoS_2/GF	0.1 M HCl	99.6 μmol cm^{-2} h^{-}	76.6	0.1 V	*Angew. Chem., Int. Ed.*, 2021, **60**, 25263–25268
Ni_2P/CP	0.1 M HCl	33.47 μmol cm^{-2} h	76.9	-0.2 V	*J. Mater. Chem. A*, 2021, **9**, 24268–24275.

Table S2. Comparison of NH_3 yields and power density of our battery with reported metal-N_2 battery systems.

Catalyst	NH_3 yield	Power density	Ref.
NiO/CP	228 μg h^{-1} cm^{-2}	0.88 mW cm^{-2}	This work
Fe 1.0 HTNs	0.172 μg $h^{-1}cm^{-2}$	0.02765 mW cm^{-2}	*J. Mater. Chem. A*, 2021, **9**, 4026–4035
CoPi/HSNPC	11.62 μg $h^{-1}mg_{cat.}^{-1}$	0.31 mW cm^{-2}	*J. Mater. Chem. A*, 2021, **9**, 11370–11380
CoPi/NPCS	14.7 μg h^{-1} $mg_{cat.}^{-1}$	0.49 mW cm^{-2}	*ACS Appl. Mater. Inter.*, 2021, **13**, 12106–12117
VN@NSC-900	0.172 μg h^{-1} cm^{-2}	0.01642 mW cm^{-2}	*Appl. Catal. B: Environ.*, 2021, **280**, 119434
Graphene/Pd	27.1 mg h^{-1} $g_{cat.}^{-1}$	/	*Energy Environ. Sci.*, 2020, **13**, 2888–2898
NbS_2	/	0.31 mW cm^{-2}	*Appl. Catal. B: Environ.*, 2020, **270**, 118892
BNFC-800	/	127 mW cm^{-2}	*J. Mater. Chem. A*, 2020, **8**, 8430–8439
Cu-2	0.125 μg h^{-1} cm^{-2}	0.0101 mW cm^{-2}	*Chem. Commun.*, 2019, **55**, 12801–12804

Table S3. Theoretical voltage for several types of metal-based batteries.

Battery type	Chemical reaction	Theoretical voltage (V)
Zn-NO	$5Zn + 2NO + 3H_2O \rightarrow 5ZnO + 2NH_3$	2.14
Li-S	$2Li + S \rightarrow Li_2S$	2.2
Li-O_2	$2Li + O_2 \rightarrow Li_2O_2$	3.0
Li-CO_2	$4Li + 3CO_2 \rightarrow C + 2Li_2CO_3$	2.7
Li-N_2	$6Li + N_2 \rightarrow 2Li_3N$	0.54
Zn-CO_2	$Zn + CO_2 + H_2O \rightarrow ZnO + HCOOH$	0.955
Al-N_2	$2Al + N_2 \rightarrow 2AlN$	0.99
Zn-Air	$2Zn + O_2 \rightarrow 2ZnO$	1.65
Zn-Nitrate	$4Zn + NO_3^- + 3H_2O \rightarrow 4ZnO + NH_4OH + OH^-$	1.85

References

1 G. Kresse and J. Hafner, *Phys. Rev. B*, 1994, **49**, 14251–14269.

2 G. Kresse and D. Joubert, *Phys. Rev. B*, 1999, **59**, 1758–1775.

3 J.P. Perdew, K. Burke and M. Ernzerhof, *Phys. Rev. Lett.*, 1996, **77**, 3865–3868.

4 H.J. Monkhorst and J.D. Pack, *Phys. Rev. B*, 1976, **13**, 5188–5192.

5 V. Wang, N. Xu, J.-C. Liu, G. Tang and W.-T. Geng, *Comput. Phys. Commun.*, 2021, **267**, 108033.

6 Y. Wang, F. Qu, J. Liu, Y. Wang, J. Zhou and S. Ruan, *Sens. Actuators, B*, 2015, **209**, 515-523.

7 L. Sui, T. Yu, D. Zhao, X. Cheng, X. Zhang, P. Wang, Y. Xu, S. Gao, H. Zhao, Y. Gao and L. Huo, *J. Hazard. Mater.*, 2020, **385**, 121570.